

Distance-based Speed Functions for Level Set Methods in Image Segmentation

Karsten Rink and Klaus Tönnies

Department of Simulation and Graphics
University of Magdeburg, Germany
karsten@isg.cs.uni-magdeburg.de

Abstract

Level set methods are a well-known means for the segmentation of objects in image data. In this paper, we discuss a class of easy to calculate terms based on distance measures for integration into the level set speed function. We will give examples for the use of these distance-based terms as a stopping criterion in the absence of reliable image features and as an acceleration force for the propagating front to connect parts of a single object. A comparison of the results with a level set segmentation not using any distance measures will be given to demonstrate the improvement of segmentation results.

1 Level Set Speed Functions

Level set methods have become popular for many domains of science as diverse as computer graphics, simulation of crystal growth or fluid mechanics. In image processing they are often used for segmentation. Because of their implicit definition level sets are independent of the number of degrees of freedom of the object of interest as well as the number of dimensions of the underlying data.

Level Sets describe the propagation process of a closed curve $C \in \mathfrak{R}^n$. This curve C is represented as the zero level set of a higher dimensional function $\Phi \in \mathfrak{R}^{n+1}$ given by

$$\Phi(\mathbf{x}, t) = \pm d, \quad (1)$$

where d denotes the distance to C . Therefore,

$$C(t) = \{\mathbf{x} | \Phi(\mathbf{x}, t) = 0\}. \quad (2)$$

C is moving in its normal direction over time. The speed of each point $\mathbf{x} \in C$ is given by a speed function F that is dependent on various internal (i.e. model-based) and external (i.e. image-based) forces. This leads to the level set equation

$$\Phi_t + F|\nabla\Phi| = 0, \quad (3)$$

where $|\nabla\Phi|$ denotes the normalised gradients of the level set function and F is the speed function. As Φ changes over time, its zero level set $\Phi(\mathbf{x}, t) = 0$ always yields the propagating front, i.e. $C(\mathbf{x})$, at time t . Depending on the application, F is defined by a number of speed terms based on the properties of the object that should be segmented.

When level sets were introduced in image segmentation, Malladi et al.[9] proposed an image-based speed term that stops the propagating front at image gradients. A model-based speed term based on local curvature results in a smooth contour and prevents leaking of the contour if image gradients are not reliable. The resulting speed function is given by

$$F = g(v + \kappa) \quad (4)$$

where v is an advection term propagating the front in normal direction, $\kappa = \nabla \frac{\nabla \Phi}{|\nabla \Phi|}$ is the curvature-based speed term and g is based on image features. The gradient-based term used in [9] is given by

$$g = \frac{1}{1 + |\nabla G_\sigma * I(x, y)|} \quad (5)$$

and results in small values at image gradients and thus stops the front at object boundaries. Prior to the calculation of gradients the image is often convolved with a Gaussian smoothing kernel G_σ to prevent the front from stopping in the presence of noise.

In a similar manner other image features (e.g. intensity distributions) may be included into the speed function, either as a factor to stop the front if the specified properties are not met or as an additive term increasing the speed independent of other forces. As an example, Caselles et al.[2] proposed a term based on the second derivatives of the image function that attracts the contour to gradients and thus makes such a segmentation process more robust.

In recent years, a large number of model- or image-based forces were proposed for various segmentation problems including speed terms into the propagation process that are based on texture [10], fuzzy decision rules[5] or shape priors [4]. Unfortunately, while these speed terms benefit the segmentation process, the resulting speed functions are often very specialised and can only be used for the application they were designed for.

In this paper, we focus on a class of distance-based forces. While these forces may not contribute as much to a segmentation process as more specialised speed terms proposed in recent years (see for instance [8, 13]), they are easy to integrate into an existing speed function, have low computational cost, are consistent with the definition of level sets and still provide valuable information.

Considering distance-based forces, we also want to mention the coupled surface approach by Zeng et al.[15] because of its relevance to one of the terms proposed in section 2. In [15] two active contours are used for the segmentation of grey and white matter in MR images of the human brain. The first contour is set to detect the boundary between grey matter and cerebrospinal fluid (CSF), the second contour to find the boundary between grey and white matter. Both contours have a speed function including a term that is zero if the distance between the contours is not in a given interval $[d_{min}, d_{max}]$. This way, both contours cannot move further apart than d_{max} or move closer to each other than d_{min} .

2 Distance-Based Speed Terms

We propose a new class of speed terms based on local distance measures. Distances in image data are easy to calculate and there are a number of segmentation problems where distance between objects or parts of objects adds information to the segmentation process.

Using the level set method, it is largely possible to avoid additional calculations. For the calculation of various speed terms (e.g. advection or curvature-based speed) a distance

transform is already performed as part of the propagation process. These calculations have to be repeated every few steps to avoid errors due to numerical approximations [9, 12]. In image processing applications distances are usually only calculated on a narrow band around the zero level set to save computational cost (see [1] for details). The surface normal n at any point of the front is given by $n = \nabla\Phi$.

We will define two classes of speed terms based on local distance measures. Class 1 will use a distance-based speed term as stopping criterion, class 2 will accelerate the propagating front if certain requirements are met within a given distance to the front.

All speed terms have a domain of $[0, 1]$ and we will demonstrate the integration of the speed terms into an existing speed function based on equation 4. Obviously, our approach is not limited to speed functions of this design and integration in other speed functions is straightforward.

2.1 A distance-based stopping term

Suppose an object X should be segmented and it is known that the boundary of X always has a minimum distance d_{min} to the boundary of a second object Y . A very simple speed function to guarantee this requirement will always be met is given by

$$F = d_s g(v + \kappa), \quad (6)$$

where g denotes image-based forces and d_s is the Heaviside step function

$$d_s = \begin{cases} 0, & \text{if } d(\mathbf{x}, \mathbf{y}) \leq d_{min}, \\ 1, & \text{otherwise.} \end{cases} \quad (7)$$

Here, $\mathbf{x} \in X$ denotes a pixel on the propagating front C and $\mathbf{y} \in Y$ is a pixel belonging to the second object. Classification is based on image features of X and Y .

Using this speed function the level set will evolve in the same way it did when using equation 4, but regardless of any image features it will keep a distance of d_{min} to Y (see figure 2(b)).

In section 3 we will give an example of an application where the contour surrounding Object X not only should keep a minimum distance d_{min} to a second object Y but also a maximum distance d_{max} .

A speed function meeting this requirement is given by

$$F = \delta g(v + \kappa) + d_s(v + \kappa), \quad (8)$$

where

$$\delta = 4d_s(1 - d_s), \quad (9)$$

with a distance-based speed term

$$d_s = \frac{d(\mathbf{x}, \mathbf{y}) - d_{min}}{d_{max} - d_{min}}. \quad (10)$$

Again, $d(\mathbf{x}, \mathbf{y})$ is the distance from $\mathbf{x} \in C$ to a pixel $\mathbf{y} \in Y$. In our experiments we only calculated distances for pixels with $d(\mathbf{x}, \mathbf{y}) < d_{max}$ which saved computational time and

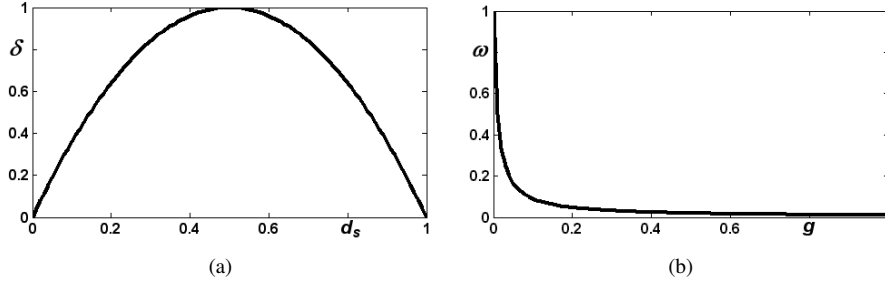


Figure 1: Plots of equation 9 and equation 14. Due to the definition of the speed terms, both functions have input and output arguments in $[0, 1]$ thus making them easily applicable to any existing speed function.

guaranteed $d_s \in [0, 1]$. To generalise this approach, equation 9 should be expanded, so that $\delta = 0$ for $d(\mathbf{x}, \mathbf{y}) > d_{max}$. Only the first term in equation 8 is dependent on image features and will vanish if $d(\mathbf{x}, \mathbf{y}) \notin [d_{min}, d_{max}]$. This way the front cannot stop if its distance from Y is greater than d_{max} . The second term is 1 if $d(\mathbf{x}, \mathbf{y}) > d_{max}$ and will decrease linearly until it reaches 0 at $d(\mathbf{x}, \mathbf{y}) = d_{min}$. That is, the smaller the distance to Y the higher the influence of the image features on the segmentation process.

The results of a segmentation using equation 8 are similar to those given in [15], although we use only one level set function and our speed function has a different design.

Finally, if $\mathbf{y} \in X$ and

$$d_s = \begin{cases} 1, & \text{if } d(\mathbf{x}, \mathbf{y}) \leq d_{max}, \\ 0, & \text{otherwise,} \end{cases} \quad (11)$$

the front will only stop at a distance d_{max} outside object X (see figure 2(d)). While equations 7 and 11 worked well with the test images, it is recommended to substitute them with sigmoid functions for the general case to avoid numerical instabilities (see [3]).

Since the given definitions guarantee $d_s \geq 0$, it is possible to integrate all the above distance-based stopping criteria into a fast marching speed function [11].

2.2 A distance-based acceleration term

In the previous section we used a distance-based measure to stop the propagating front. Now we will give an example of a speed term that pushes the front forward even if image features suggest that it should be stopped.

This property may be used if parts of a single object appear to be disconnected in the image data. For instance, thin structures (e.g. vessels) in 3D data sets are often disconnected due to partial volume effects (PVE). During segmentation these disconnected parts might either be missed or it requires additional effort to segment them in a postprocessing step.

To overcome this limitation, a term d_a is calculated based on pixels along the surface normals of the propagating front C . If a pixel \mathbf{y} within a given distance of C has the properties of the currently segmented object and $\Phi(\mathbf{y}) > 0$, the propagating front will be pushed towards this pixel. Since this search process is based on the surface normal, the

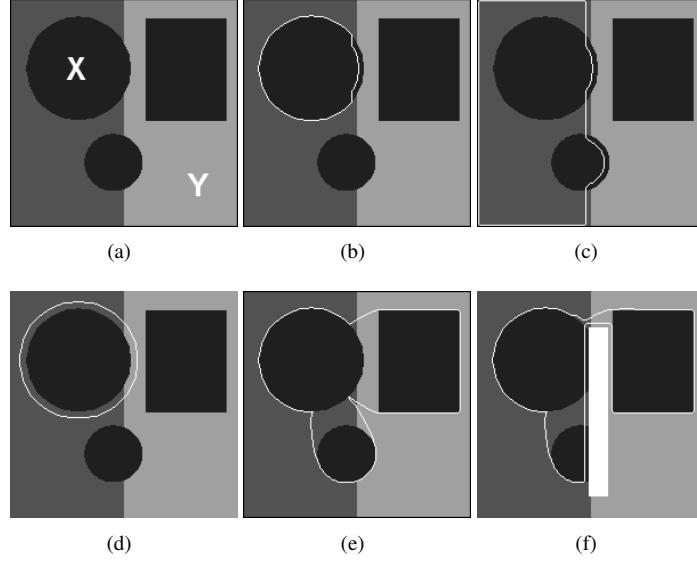


Figure 2: Figure 2(a) shows a test image to visualise the effects of distance-based speed terms. In all examples the same parameters for image-based forces have been used and a single seed point was set within object X . Figure 2(b) shows a segmentation using the minimum-distance speed term given in equation 7. The level set stops based on image-features but keeps a minimum distance of 5 pixels to the light grey area (object Y). In figure 2(c) the speed function from equation 8 was used, incorporating the min/max distance. The front does not stop at the boundary of the circle because the distance to object Y is too large. Figure 2(d) shows a segmentation using equation 11. The front stops 5 pixels outside object X . Figure 2(e) visualises the segmentation result using the acceleration term given in equation 12. All the black objects have been connected. Note, that the front propagated directly from X to the other objects and does not leak into the image background. Finally, figure 2(f) combines both approaches. The black objects are connected while the front keeps a distance of 5 pixels to the white rectangle.

distance between object parts (i.e. the distance where no reliable data for the segmentation exists) will be as small as possible.

The resulting level set speed function is now given by

$$F = g(\mathbf{v} + \kappa) + \omega d_a \mathbf{v}. \quad (12)$$

The term $d_a = d_a(\mathbf{x})$ is calculated based on the image features of pixels \mathbf{y} along the surface normal of \mathbf{x} , i.e.

$$d_a(\mathbf{x}) = \max_{d_{min} \leq \mathbf{y} \leq d_{max}} g(\mathbf{y}), \quad \Phi(\mathbf{y} > 0) \quad (13)$$

and

$$\omega = \alpha(\alpha + g)^{-1}. \quad (14)$$

If the image features represented by g suggest that the front should be stopped, the second term may nevertheless add speed to the front pixel if there are pixels along the

normal that seem to belong to the object. If the value of g is high, ω will vanish, so no additional force will be applied. The parameter α determines how small g needs to be before the distance-based term add increases the speed of the front. In our experiments we used $\alpha = 0.01$ (see figure 1(b)).

Note, that due to the discrete representation of the front C relevant pixels may not be found on the surface normal of any front pixel. Therefore, for implementation purposes, we calculate d_a for all pixels \mathbf{y} within a given distance d_{max} that have not yet been segmented (i.e. $\Phi(\mathbf{y}) > 0$). A pixel is considered only if

$$d(\mathbf{x}, \mathbf{y}) - d(C, \mathbf{y}) < \epsilon. \quad (15)$$

Here, $d(\mathbf{x}, \mathbf{y})$ denotes the distance between $\mathbf{x} \in C$ and \mathbf{y} and $d(C, \mathbf{y})$ is the shortest path from \mathbf{y} to the propagating front, automatically given by the distance transform of the level set method (see beginning of this section).

3 Applications and Experimental Results

In this section we will give examples of applications for the proposed speed terms. Level set methods have been applied for the segmentation of 3D data sets using the speed function from equation 4 as well as a speed function containing the distance-based terms introduced in section 2. Results of both segmentation processes will be given for comparison.

3.1 Segmentation of Cerebral White Matter

We used the distance-based stopping criterion for the segmentation of white matter in magnetic resonance (MR) images of the human brain. The grey matter of the cerebral cortex surrounding the white matter is known to have a thickness of $2 - 6\text{mm}$ (see for instance [7, 6]). The whole brain in turn is embedded into cerebrospinal fluid (CSF). Due to inhomogeneities, partial volume effects and noise, the inner cortical surface (i.e. the boundary between the grey and white matter) is often not clearly distinguishable. Also, the magnitude of the gradients between grey and white matter varies significantly. On the other hand, the outer cortical surface is very prominent and the CSF itself is represented by much smaller image intensities in T1-weighted MRI than any brain tissue.

As it is difficult to identify the inner cortical surface, anatomical knowledge of cortex thickness can be used as a constraint in the segmentation process. Using the level set method, the propagating front should be stopped if the distance between white matter and CSF is less than 2mm , even if there is no discernable boundary between grey and white matter visible within the data. Also, the front cannot be stopped if it is more than 6mm away from voxels classified as CSF.

In the scope of this paper we just want to give the different results for a segmentation of the white matter with and without our stopping criterion. Note, that we did not perform skull stripping or any other preprocessing steps. Rough estimates for white matter and CSF distributions were obtained by placing one seed point within the respective tissue and then start a very conservative segmentation using the fast marching method (see fig. 3(b)). A more sophisticated histogram analysis will improve results (see [14]) but is not performed here. Instead, we want to focus on the benefit of the distance-based criterion with respect to the cortical surface estimation.

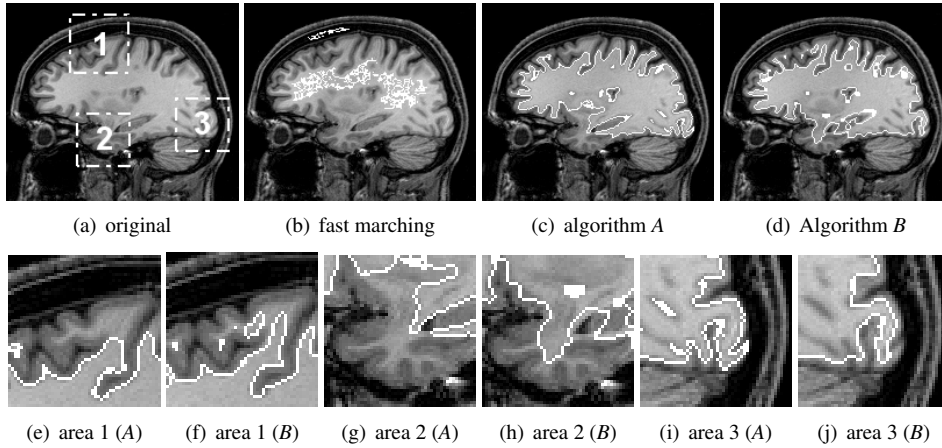


Figure 3: Segmentation of white matter in MR data of the human brain. Figure 3(b) shows the result of a conservative fast marching segmentation to obtain mean value and standard deviation for white matter and CSF. Figure 3(c) shows the segmentation result using algorithm *A*, figure 3(d) shows the segmentation result using algorithm *B*. Note the differences in the marked areas, enlarged in figs 3(e)–3(j).

We tested our speed function on five 3 Tesla MRI data sets of the human brain with a resolution of 1mm^3 iso-voxels. We will refer to the segmentation without the stopping criterion as algorithm *A* and to the segmentation including the stopping criterion as algorithm *B*. The same parameter set was used for both segmentation processes. Segmentation results obtained with both algorithms are presented in figure 3. Due to magnetic field inhomogeneities, algorithm *A* misses white matter pixels in the upper frontal lobe (area 1) and in the lower temporal lobe (area 2). In area 3, voxels belonging to the cortex have been misclassified as white matter. Using algorithm *B* resulted in an improved result. Additional white matter pixels are segmented in areas 1 and 2 due to the maximum allowed distance d_{max} to CSF, less pixels are segmented in area 3 due to the minimum required distance d_{min} to CSF.

We are aware that segmentation results for algorithm *A* can be improved using appropriate preprocessing steps. The same is true for algorithm *B*, as segmentation near the cortex is still governed by the image-based speed terms (see equation 8). Furthermore, segmentation using algorithm *B* proved to be much more robust since including the stopping criterion prevents the propagating front from leaking into non-white matter if image-based forces are too small. At the same time, the front cannot stop somewhere within the white matter if image-based forces are too strong. An evaluation and comparison of the method to other algorithms would go beyond the scope of this paper. Instead, we refer the reader to [14] where we applied a similar method based on region growing to 1.5 Tesla MR images of the human brain. The proposed algorithm includes a number of preprocessing steps to ensure robust segmentation as well as an evaluation by experts. Results proved to be more exact than those of the commercial software BrainVoyager.

data set	1	2	3	4	5
# spines	27	28	37	19	25
algorithm <i>A</i>	7	8	16	5	8
algorithm <i>B</i>	21	16	23	17	18

Table 1: Segmentation of spines for five dendrites. Given are the number of spines for each dendrite as well as the number of spines found using a level set algorithm without the acceleration term (algorithm *A*) and with the acceleration term (algorithm *B*).

3.2 Segmentation of Dendrites

A speed term accelerating the front even if image features suggest that the front should be stopped, can be used to connect parts of an object that appear to be disconnected in the data. The speed function given in equation 12 connects different objects (or parts of an object) if the distance between them is small enough and they have similar image features. We applied this speed function for the segmentation of branches of neurons, called dendrites, in 3D microscopic images. The synapses by which different neurons send signals to each other are located either on the dendrites themselves or on small extensions (spines) of the dendrites. For research of neural processing a segmentation of these structures is necessary. Unfortunately, spines often seem unconnected to dendrites due to partial volume effects which makes a segmentation of these structures difficult.

Our method was tested on three microscopic data sets with $1\mu m^3$ iso-voxels. The maximum response criterion in equation 13 poses a problem in the presence of high noise levels as the front tends to be pushed towards single noise pixels. Therefore, the data was smoothed using a small gaussian kernel. Again, we used the same parameter set in all segmentations. Parameters used for the calculation of d_a in equation 13 were $d_{min} = 1$ and $d_{max} = 12$. Therefore we missed spines at greater distance. However, setting d_{max} to a larger value may result in the connection of semantically independent objects (i.e. parts of other dendrites) as the speed of the front is based solely on image features.

In figure 4 we give examples of our segmentation results as well as comparisons of the same data set segmented using a speed function without distance-based forces. It can be seen that while we could not find all spines extending from the dendrites, we were able to segment considerably more spines using the distance-based speed term than using a conventional speed function. Unfortunately, no gold standard for an exact segmentation was available. In table 1 we give a comparison of results based on the number of segmented spines to demonstrate the benefit of the proposed acceleration term. The image intensities of the missed spines are often too low for the estimated intensity distribution of the dendrite, which was at least in part promoted by the smoothing process.

4 Conclusions

We presented a number of speed terms for a level set speed function based on local distance measures. These force terms are easy to calculate and they use local distance information from the level set itself. They can be integrated in any existing speed function and only influence the speed function when in their defined range. This way they may add

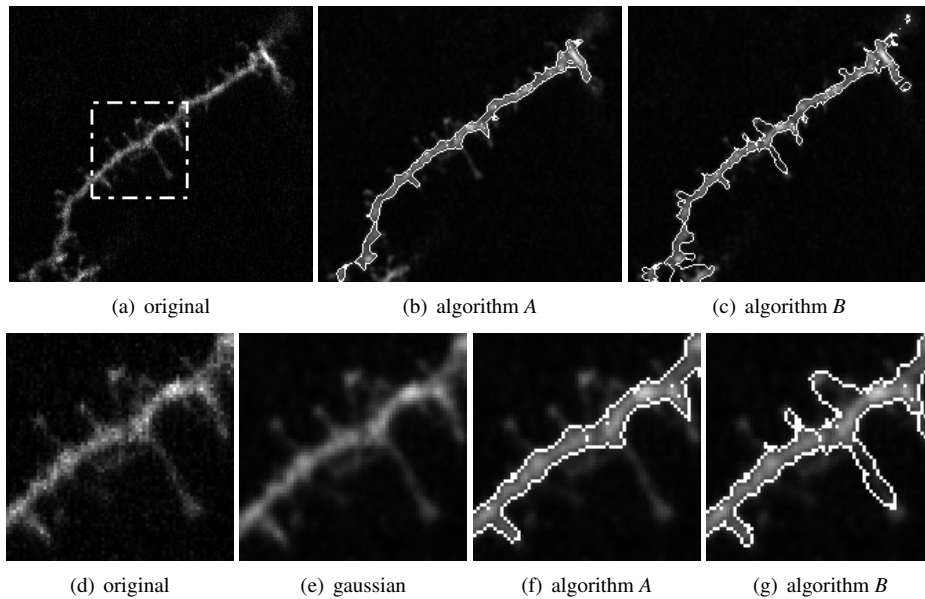


Figure 4: The upper row shows an example slice from one data set. Algorithm *A* is the segmentation without the proposed acceleration term (fig. 4(b)) and algorithm *B* is the segmentation with the acceleration term (fig. 4(c)). A number of spines that have been missed by *A* could be segmented using *B*. The lower row gives a detailed view.

valuable information to the segmentation process.

The speed terms were used in example applications for segmentation of medical data. A distance-based stopping term was applied for the segmentation of cerebral white matter in 3D MR data sets of the human brain to ensure a semantically correct estimation of the inner cortical surface in the absence of reliable image features. A distance-based acceleration term was used for the segmentation of dendrites in 3D microscopic images to connect parts of the segmented object that appear disconnected due to partial volume effects. In both cases segmentation results have been improved when compared to a conventional level set segmentation using the same parameter sets. Also, segmentation results using the stopping criterion proved to be more robust to parameter variations. A way to handle the noise-dependence of the acceleration force will be investigated in future work.

Acknowledgements

We would like to thank Karin Engel and Christian Wasserthal for the discussions as well as the Leibniz Institute for Neurobiology, Magdeburg, for the data sets.

References

- [1] D. Adalsteinsson and J. A. Sethian. A Fast Level Set Method for Propagating Interfaces. *J Comput Phys*, 118(2):269–277, 1995.
- [2] V. Caselles, R. Kimmel, and G. Sapiro. Geodesic Active Contours. *Int J Comput Vis*, 22(1):61–79, 1991.
- [3] T. F. Chan and L. A. Vese. Active Contours Without Edges. *IEEE Trans Imag Proc*, 10(2):266–277, 2001.
- [4] Y. Chen, S. Thiruvenkadam, H. D. Tagare, F. Huang, D. Wilson, and E. A. Geiser. On the Incorporation of shape priors into geometric active contours. In *Proc of the IEEE Workshop on Variational, Geometric and Level Set Methods in Computer Vision*, pages 145–152, 2001.
- [5] C. Ciofolo. Atlas-Based Segmentation Using Level Sets and Fuzzy Labels. In *Proc of MICCAI*, pages 310–317, 2004.
- [6] C. V. Economo. *The Cytoarchitectonics of the Human Cerebral Cortex*. Oxford University Press, 1929.
- [7] B. Fischl and A. M. Dale. Measuring the thickness of the human cerebral cortex from magnetic resonance images. *Proc Natl Acad Sci*, 97:11050–11055, 2000.
- [8] M. E. Leventon, W. E. L. Grimson, and O. Faugeras. Statistical Shape Influence in Geodesic Active Contours. In *Proc of IEEE Conference on Computer Vision and Pattern Recognition*, pages 316–322, 2000.
- [9] R. Malladi, J. A. Sethian, and B. Vemuri. Shape Modelling with Front Propagation: A Level Set Approach. *IEEE Trans Pattern Anal Mach Intell*, 17(2):158–175, 1995.
- [10] N. Paragios and R. Deriche. Geodesic Active Contours and Level Sets for the Detection and Tracking of Moving Objects. *IEEE Trans Pattern Anal Mach Intell*, 22(3):266–280, 2000.
- [11] J. A. Sethian. A Fast Marching Level Set Method for Monotonically Advancing Fronts. *Proc Natl Acad Sci*, 93(4):1591–1595, 1996.
- [12] J. A. Sethian. *Level Set Methods and Fast Marching Methods*. Cambridge University Press, 1999.
- [13] C. M. van Bommel, L. J. Spreeuwiers, M. A. Viergever, and W. J. Niessen. A Level-Set-Based Artery-Vein Separation in Blood-Pool Agent CR-MR Angiograms. *IEEE Trans Med Imag*, 22(10):1224–1234, 2003.
- [14] C. Wasserthal, K. Engel, K. Rink, and A. Brechmann. Automatic Segmentation of the Cortical Grey and White Matter in MRI Using a Region Growing Approach Based on Anatomical Knowledge. In *Proc of Bildverarbeitung für die Medizin*, pages 437–441, 2008.
- [15] X. Zeng, L. H. Staib, R. T. Schultz, and J. S. Duncan. Segmentation and Measurements of the Cortex from 3-D MR Images Using Coupled-Surfaces Propagation. *IEEE Trans Med Imag*, 18(10):927–937, 1999.